NASA TN D-1628

TECHNICAL NOTE

D-1628

PRESSURE AND HEAT-TRANSFER MEASUREMENTS ON THE FLAT FACE OF A BLUNTED 10° HALF-CONE BODY (SEMIDISK) AT A MACH NUMBER OF 6.15

By P. Calvin Stainback

Langley Research Center
Langley Station, Hampton, Va.

NATIONAL AERONAUTICS AND SPACE ADMINISTRATION
WASHINGTON

May 1963

NATIONAL AERONAUTICS AND SPACE ADMINISTRATION

TECHNICAL NOTE D-1628

PRESSURE AND HEAT-TRANSFER MEASUREMENTS ON THE FLAT FACE OF A BLUNTED 10° HALF-CONE BODY (SEMIDISK) AT A MACH NUMBER OF 6.15

By P. Calvin Stainback

SUMMARY

An experimental investigation was conducted to evaluate the flow characteristics of the front face of a 10° half-cone blunted approximately 85 percent with respect to the base radius. The front face was flat and inclined at an angle of 60° with respect to the original axis of the cone. The instrumented portion of the model was essentially a semidisk. Tests were conducted at a nominal Mach number of 6.15 and a nominal stagnation temperature of 450° F for an angle-of-attack range of 0° to 60°. The test-section Reynolds number was varied from 0.67×10^6 to 5.25×10^6 per foot for the heat-transfer tests and was 6.92×10^6 per foot for the pressure tests.

The results indicated that the pressure and heat-transfer characteristics of the front face, at all angles of attack, were qualitatively similar to those of a disk normal to the free-stream velocity. The stagnation-point location was found to vary approximately linearly with angle of attack in the range investigated. The average heat-transfer coefficient over the face was essentially constant for the angle-of-attack range of this investigation and approximately equal to the average coefficient of a disk situated normal to the free-stream velocity.

INTRODUCTION

Manned orbital and superorbital flight studies have given rise to a group of lifting-body configurations with limited lift-drag ratios and lifting capabilities. In order to reduce the stagnation-point heating, to increase the lift, and to trim the body at the proper attitude, several investigators have recommended blunting the basic body shape and canting the nose. (For example, see refs. 1, 2, and 3.) This alteration of the body often results in a nose that is relatively flat, and at the design attitude the flat face is almost normal to the free-stream velocity. Consequently, the prediction of heating to the nose, which can be high, cannot be made with great certainty. It is the purpose of this paper to present some preliminary data taken on the flat-face, sharp-corner nose of an ungular 10° half-cone. The aforementioned data consist of flow-visualization studies (schlieren, oil flow, and temperature-sensitive paint) and pressure and

heat-transfer measurements. The heat-transfer characteristics of complete vehicles utilizing the canted-nose concept can be found in references 4 and 5.

SYMBOLS

b	vertical height of nose
d	disk diameter
h_t	theoretical stagnation-point heat-transfer coefficient of a disk normal to free-stream velocity
h	local-heat-transfer coefficient
$\bar{H}$	average heat-transfer coefficient
M	Mach number
p	local static pressure
p_t	free-stream stagnation pressure
p_t'	stagnation pressure behind a normal shock
r_b	base radius
r_m	radial distance from midpoint of lower edge of model
r_n	larger radial dimension of nose
T_t	stagnation temperature
T_w	wall temperature
α	angle of attack
θ	angular distance from lower surface of model (see fig. 1)
θ'	angular distance from thermocouple row located parallel to lower surface of model (see fig. 1)

MODEL, TEST PROCEDURE, AND RECORDING AND REDUCTION OF DATA

Model

The model was basically a 10° half-cone which was blunted approximately 85 percent with respect to the base radius, by passing a plane through the half-cone at an angle of 60° with respect to the center line of the original cone. A drawing of the model is presented in figure 1. The heat-transfer model was fabricated from 0.034-inch-thick stainless steel and was instrumented with 15 iron-constantan thermocouples. The pressure model, constructed of 0.050-inch-thick stainless steel, was instrumented with 15 pressure orifices which were 0.040 inch in diameter. (See fig. 1.) The oil-flow and temperature-sensitive-paint models were made from solid aluminum and high-temperature plastic, respectively. All corners were relatively sharp with respect to the general dimensions of the model. Although the model was basically a cone, the alterations made resulted in an instrumented surface that was essentially one-half of a disk. Actually, the nose is a portion of an ellipse, and the ratio of the larger radial dimension to the smaller one is 1.048. Because of this, the data approximate that for a semidisk where the angle of attack varies ±30° from the attitude where the face is normal to the free-stream direction. In the following discussion, the nose dimension r_n is considered as the radius of the nose whereas in reality it is the larger dimension of the nose.

Test Procedure and Recording and Reduction of Data

The models were tested in a 12- by 14-inch blowdown jet at the Langley Research Center at a nominal Mach number of 6.15 and a nominal stagnation temperature of 450° F. The test-section Reynolds number was varied from 0.67×10^6 to 5.25×10^6 per foot for the heat-transfer test and was 6.92×10^6 per foot for the pressure and flow-visualization tests.

The heat-transfer model was tested by the transient-heating method by starting the tunnel with the model outside the test section and injecting the model into the airstream after steady operation was obtained. For details on the method of recording and reducing the heat-transfer data, see reference 6. The heat-transfer coefficient was nondimensionalized by dividing the local-heat-transfer coefficient by the theoretical stagnation-point heat-transfer coefficient of a disk situated normal to the free-stream velocity and having an area equal to that of the flat nose of the test model. The ratio of the stagnation-point heat-transfer coefficient for a disk to that of a sphere of the same diameter was taken to be 0.56. (See ref. 7.) The stagnation-point heat-transfer coefficient was calculated by the method of reference 8. The recovery temperature was assumed to be equal to the stagnation temperature since the pressure data indicated that the recovery temperature, calculated from measured pressures with the assumption of isentropic flow from the stagnation point, was essentially equal to the stagnation temperature.

The model pressures were measured with a Statham pressure transducer having a range of 0 to 15 psia. The oil-flow and temperature-sensitive-paint investigations were conducted in a manner similar to that of the heat-transfer test. Reference 9 describes the temperature-sensitive-paint testing technique in some detail.

DISCUSSION OF RESULTS

Flow-Visualization Studies

Typical photographs of the results obtained with the oil-flow and temperature-sensitive-paint techniques and a schlieren system are presented in figures 2 to 5.

The oil-flow tests were used to obtain approximate stagnation-point locations for the various angles of attack investigated. These results are shown in figure 6. This figure indicates that the stagnation point is very near the "leading edge" at angles of attack of 0° and 60° and that the variation of the stagnation-point location between these angles is essentially linear.

The stagnation point should be at $r_m/r_n = 0$ for an angle of attack of 60°, but a close examination of the oil dots located in the vicinity of $r_m/r_n = 0$ revealed some oil flow around the corner from the face to the lower portion of the body. Whether this is due to gravitational effects or the testing technique (i.e., injection and retraction of the model into and from the test section) is not known. If the flow is assumed to be locally two dimensional, the shock should become attached to the body at $\alpha = -17.5^\circ$, and this position can be considered the end point for the stagnation-point location. With this assumption, the stagnation point would have little movement with a change in α from -17.5° to 0°. The flat face is normal to the free-stream velocity at $\alpha = 30^\circ$, and at this angle of attack the stagnation point is approximately at the midpoint of the vertical center line although the model is not symmetrical.

Test results of oil flow over a flat-face body of revolution (a disk) at various angles of attack and at a Mach number of 8 are presented in figure 3. The stagnation-point location for the disk, which was determined from the oil-flow studies and agrees with that determined from pressure tests, is presented in figure 6. The results indicated that the movement of the stagnation-point location with angle of attack for the flat face of the cone is similar to that for the disk, but the stagnation-point variation is somewhat more linear for the cone than for the disk.

The darker (actual color - black) regions of the model in figure 4, which shows the temperature-sensitive-paint test results, indicate higher heating rates than the lighter (actual color - blue) regions. These results verify the expected high heating rates along the periphery of the nose and indicate, in general, that the highest heating rates at the periphery were along the edge nearest the stagnation point. The temperature-sensitive-paint results are compatible with the heat-transfer results presented in a subsequent section.

Pressure Data

The pressure data are presented in figure 7 as lines of constant pressure for the angles of attack investigated. These lines were obtained by plotting the data of table I as a function of r_m/r_n for constant values of θ' and as a function of θ for constant values of r_m/r_n. These two sets of faired curves were made to be consistent and to agree with the data, and to give reasonable contours for the lines of constant pressure. The stagnation point was outside the instrumented area for angles of attack of 0°, 10°, 50°, and 60°. The curves for these angles of attack were constructed by using the stagnation-point location obtained from the oil-flow investigation. The sonic line was assumed to be located at the periphery of the model for all conditions investigated except for the "leading edge" $\left(r_m/r_n = 0\right)$ at $\alpha = 60^\circ$.

The pressure results for the disk obtained at a Mach number of 8 (from ref. 10) are presented in figure 8. The pressure results for both configurations are qualitatively similar to the results obtained for the disk situated normal to the free-stream velocity ($\alpha = 0^\circ$). That is, the pressure is roughly constant over a large portion of the surface, but it decreases rapidly along the periphery of the face. The asymmetry of the blunt cone and angle of attack, of course, results in an asymmetric pressure distribution over the models. Deviations from these general results increased with α. It should be noted that the shock is apparently attached to the disk at an angle of attack of 45°, and this probably caused the marked difference between the pressure contours at $\alpha = 30^\circ$ and those at $\alpha = 45^\circ$.

The size of the model limited the amount of instrumentation which could be used and precludes an evaluation of the velocity gradient at the stagnation point.

Heat-Transfer Data

The heat-transfer data for a Reynolds number of 5.25×10^6 per foot are presented in figure 9 as lines of constant heat-transfer coefficient for the angles of attack investigated. These curves were obtained in a manner similar to that used for plotting the pressure data. Data for all Reynolds numbers investigated are included in table II. Heat-transfer results for the disk are shown in figure 10 (from ref. 10).

The heat-transfer results for the test model, like the pressure results, are qualitatively similar to the results obtained for the disk. That is, the heating is roughly constant over a large portion of the surface, but there is a significant increase at the periphery of the instrumented face. The deviation from these general results with increased angle of attack is more pronounced for the disk than for the blunt cone. This deviation is manifested by the ratio of the maximum heating rate to the minimum rate which is much greater for the disk than for the blunt cone. Nonsymmetric heating rates occur as a result of the asymmetry of the model and angle of attack. The high heating rates along the periphery are greatest in the vicinity of the stagnation point, and this result is compatible with the pressure and the temperature-sensitive-paint results.

Because of the limited pressure instrumentation, a comparison of the data with theory could not be made. In order to obtain some quantitative comparison between the heating rates for the present model and similar configurations, the average heat-transfer coefficients over the front faces of the blunt cone and the disk were calculated and are shown in figure 11. The data of figure 11 indicate that the average heating for the blunt cone is approximately constant over the angle-of-attack range investigated and approximately equal to the average coefficient of a flat-face disk situated normal to the free-stream velocity, whereas the average heating for the disk decreased about 15 percent over this same angle-of-attack range.

CONCLUDING REMARKS

The flow characteristics of the flat face of a blunted 10° half-cone indicated that the pressure and heat-transfer distributions were qualitatively similar to those of a disk but included some asymmetry due to the asymmetry of the model and angle of attack. The location of the stagnation point was found to vary almost linearly with angle of attack over the range investigated. The average heat-transfer coefficient was constant over the angle-of-attack range of this investigation and had a value approximately equal to that for a disk normal to the free-stream velocity.

Langley Research Center,
National Aeronautics and Space Administration,
Langley Station, Hampton, Va., January 14, 1963.

REFERENCES

1. Davy, William C., and Seiff, Alvin: A Study of the Stability and Performance of Some Unsymmetrical Truncated Conical Configurations for Lifting Re-entry. NASA TM X-504, 1961.

2. Armstrong, William O.: Hypersonic Aerodynamic Characteristics of Several Series of Lifting Bodies Applicable to Reentry Vehicle Design. NASA TM X-536, 1961.

3. Armstrong, William O.: Aerodynamic Characteristics of a Flat-Bottom Canted-Nose Half-Cone Reentry Configuration at a Mach Number of 6.7. NASA TM X-630, 1962.

4. Coe, Frank S., III, and Feller, William V.: Experimental Investigation of the Pressures, Heat Transfer, and Surface Flow Patterns Around a Blunt Half-Cone Lifting Reentry Body at a Mach Number of 9.6. NASA TM X-589, 1961.

5. Terry, James E.: Convective Heat Transfer to a Lifting Flat-Faced-Cone Entry Body. NASA TM X-509, 1961.

6. Stainback, P. Calvin: Heat-Transfer Measurements at a Mach Number of 4.95 on Two 60° Swept Delta Wings With Blunt Leading Edges and Dihedral Angles of 0° and 45°. NASA TN D-549, 1961.

7. Cooper, Morton, and Mayo, Edward E.: Measurements of Local Heat Transfer and Pressure on Six 2-Inch-Diameter Blunt Bodies at a Mach Number of 4.95 and at Reynolds Numbers Per Foot up to 81×10^6. NASA MEMO 1-3-59L, 1959.

8. Reshotko, Eli, and Cohen, Clarence B.: Heat Transfer at the Forward Stagnation Point of Blunt Bodies. NACA TN 3513, 1955.

9. Stainback, P. Calvin: A Visual Technique for Determining Qualitative Aerodynamic Heating Rates on Complex Configurations. NASA TN D-385, 1960.

10. Jones, Robert A.: Heat-Transfer and Pressure Distributions of Two Flat-Face Sharp-Corner Bodies of Revolution at a Mach Number of 8 and Comparison With Data for a Round-Corner Body. NASA TM X-774, 1963.

TABLE I.- PRESSURE DATA

Orifice	$\frac{r_m}{r_n}$	θ', deg	θ, deg	p/p_t' for α of -						
				0°	10°	20°	30°	40°	50°	60°
1	0.246	----	90	0.7636	0.8447	0.8843	0.9438	0.9278	0.9499	0.9452
2	.342	0	45.99	.7635	.8452	.8886	.9447	.9364	.9551	.9429
3	.536	0	27.37	.7509	.8310	.8697	.9260	.9193	.9397	.9199
4	.755	0	19.04	.7396	.8125	.8596	.9075	.9065	.9068	.8813
5	.342	45	75.57	.7880	.8705	.9076	.9529	.9350	.9454	.9222
6	.536	45	63.97	.8156	.8895	.9097	.9421	.9068	.9026	.8571
7	.755	45	58.34	.8421	.8967	.9030	.9150	.8808	.8454	.7958
8	.536	90	90	.8332	.9047	.9195	.9451	.8972	.8962	.8468
9	.755	90	90	.8794	.9229	.9249	.9193	.8686	.7554	.7897
10	.342	67.5	83.48	.7892	.8737	.9076	.9543	.9266	.9439	.9174
11	.536	67.5	77.63	.8402	.9130	.9391	.9557	.9313	.9121	.8616
12	.755	67.5	74.67	.8772	.9237	.9231	.9153	.7700	.8529	.7880
13	.342	22.5	64.15	.7819	.8641	.9022	.9505	.9272	.9482	.9290
14	.536	22.5	47.63	.8053	.8848	.9201	.9532	.9199	.9330	.8958
15	.755	22.5	40.04	.8048	.8699	.8942	.9178	.8662	.8745	.8225

α, deg	0	10	20	30	40	50	60
p_t, psig	445	445	450	446	447	449	444
T_t, °F	469	468	465	466	459	464	466

TABLE II.- HEAT-TRANSFER DATA

Thermocouple	$\frac{r_n}{r_m}$	θ'	α = 0°				α = 10°						α = 20°						α = 30°					
			p_t = 149 psig, T_t = 396° F		p_t = 300 psig, T_t = 485° F		p_t = 25.5 psig, T_t = 320° F		p_t = 150 psig, T_t = 365° F		p_t = 300 psig, T_t = 375° F		p_t = 25 psig, T_t = 320° F		p_t = 150 psig, T_t = 400° F		p_t = 300 psig, T_t = 455° F		p_t = 25 psig, T_t = 360° F		p_t = 140 psig, T_t = 450° F		p_t = 300 psig, T_t = 505° F	
			h (a)	T_w, °F	h (a)	T_w, °F	h (a)	T_w, °F	h (a)	T_w, °F	h (a)	T_w, °F	h (a)	T_w, °F	h (a)	T_w, °F	h (a)	T_w, °F	h (a)	T_w, °F	h (a)	T_w, °F	h (a)	T_w, °F
1	0.246	----	0.00812	87	0.01123	96	0.00512	81	0.00913	90	0.01232	78	0.00488	82	0.01099	93	0.01388	84	0.00628	91	0.01196	105	0.01751	115
2	.342	0	.00831	91	.01207	104	.00519	79	.00977	91	.01335	78	.00575	84	.01147	93	.01484	85	.00657	91	.01304	106	.01794	116
3	.536	0	.00998	92	.01277	97	.00563	79	.01029	91	.01486	79	.00661	84	.01168	89	.01708	94	.00767	92	.01445	107	.01809	116
4	.755	0	.01123	92	.01506	105	.00656	81	.01157	87	.01603	85	.00638	82	.01328	94	.01797	94	.00740	91	.01442	106	.01852	115
5	.342	45	.00821	87	.01110	103	.00473	79	.00895	90	.01163	83	.00504	83	.01020	93	.01365	91	.00564	91	.01143	104	.01663	105
6	.536	45	.00930	91	.01256	103	.00574	81	.00932	91	.01288	83	.00540	83	.01118	93	.01477	91	.00604	90	.01117	103	.01521	113
7	.755	45																						
8	.342	90	.00713	87	.01072	102	.00429	79	.00854	90	.01113	82	.00443	81	.00973	88	.01361	91	.00609	90	.01162	98	.01595	113
9	.536	90	.00772	90	.01005	101	.00524	79	.00953	87	.01255	83	.00497	81	.00851	91	.01121	89	.00539	87	.00919	101	.01336	111
10	.755	90	.01163	89	.01720	108	.00668	81	.01237	93	.01667	86	.00658	84	.01274	94	.01775	94	.00658	88	.01208	98	.01635	114
11	.536	67.5	.00827	91	.01129	102	.00512	80	.00883	87	.01203	82	.00500	83	.00987	92	.01208	83	.00541	88	.01061	103	.01460	112
12	.755	67.5	.01135	93	.01549	105	.00623	81	.01124	91	.01526	84	.00623	83	.01101	92	.01528	91	.00527	90	.01077	102	.01499	112
13	.342	22.5	.00774	87	.01120	102	.00427	79	.00904	87	.01189	82	.00510	81	.00990	92	.01412	91	.00565	91	.01166	104	.01623	114
14	.536	22.5	.00866	91	.01187	103	.00516	81	.00936	87	.01288	83	.00538	82	.01044	93	.01419	91	.00592	90	.01156	104	.01516	114
15	.755	22.5	.01200	94	.01648	107	.00694	81	.01218	93	.01676	86	.00718	84	.01195	89	.01762	94	.00667	88	.01282	98	.01686	115

[a] h given in Btu/(sec)(sq ft)(°F).

TABLE II.- HEAT-TRANSFER DATA - Concluded

Thermocouple	$\frac{r_n}{r_m}$	θ'	α = 40°						α = 50°						α = 60°					
			p_t = 24 psig, T_t = 380° F		p_t = 150 psig, T_t = 490° F		p_t = 300 psig, T_t = 500° F		p_t = 25 psig, T_t = 365° F		p_t = 150 psig, T_t = 425° F		p_t = 300 psig, T_t = 400° F		p_t = 24.5 psig, T_t = 365° F		p_t = 25 psig, T_t = 425° F		p_t = 300 psig, T_t = 420° F	
			h (a)	T_w, °F	h (a)	T_w, °F	h (a)	T_w, °F	h (a)	T_w, °F	h (a)	T_w, °F	h (a)	T_w, °F	h (a)	T_w, °F	h (a)	T_w, °F	h (a)	T_w, °F
1	0.246	----	0.00612	90	0.01389	105	0.01794	122	0.00707	91	0.01352	92	0.01917	87	0.00668	96	0.00839	98	0.01837	88
2	.342	0	.00662	90	.01458	106	.01823	123	.00746	91	.01361	92	.01918	87	.00668	96	.00880	98	.01865	88
3	.536	0	.00752	90	.01516	107	.01918	124	.00784	91	.01500	93	.02085	88	.00704	97	.00935	99	.02023	89
4	.755	0	.00729	90	.01479	106	.01868	122	.00785	91	.01402	91	.01955	86	.00713	96	.00908	98	.01825	88
5	.342	45	.00550	89	.01277	104	.01654	121	.00631	91	.01204	91	.01698	86	.00573	96	.00781	98	.01617	87
6	.536	45	.00546	89	.01106	103	.01472	118	.00600	90	.01098	90	.01425	83	.00491	96	.00787	98	.01447	86
7	.755	45																		
8	.342	90	.00561	89	.01216	104	.01561	120	.00623	90	.01177	91	.01621	85	.00579	96	.00775	98	.01595	86
9	.536	90	.00370	87	.00802	100	.01209	115	.00452	89	.00871	89	.01158	82	.00360	95	.00485	97	.01127	85
10	.755	90	.00545	89	.01116	102	.01576	117	.00540	90	.01127	90	.01472	84	.00452	95	.00798	99	.01289	86
11	.536	67.5	.00486	88	.01047	102	.01461	117	.00513	90	.01001	89	.01409	83	.00458	95	.00763	98	.01251	85
12	.755	67.5	.00474	88	.01023	101	.01393	115	.00481	89	.00952	89	.01354	82	.00413	95	.00693	98	.01124	84
13	.342	22.5	.00602	89	.01268	104	.01702	121	.00633	90	.01245	91	.01780	85	.00610	96	.00789	98	.01600	87
14	.536	22.5	.00543	89	.01184	103	.01575	119	.00618	90	.01142	90	.01569	84	.00524	96	.00766	98	.01477	86
15	.755	22.5	.00612	89	.01258	104	.01673	120	.00608	90	.01189	91	.01586	84	.00538	95	.00798	99	.01473	87

[a] h given in Btu/(sec)(sq ft)(°F).

Station	r_m	θ	θ'	Thermo-couple	Press. orifice
1	.234	90	—	1	1
2	.325	46	0	2	2
3	.509	27	0	3	3
4	.717	19	0	4	4
5	.325	76	45	5	5
6	.509	64	45	6	6
7	.717	58	45	7	7
8	.325	90	90	8	8
9	.509	90	90	9	9
10	.717	90	90	10	—
11	.325	83	67.5	—	10
12	.509	78	67.5	11	11
13	.717	75	67.5	12	12
14	.325	64	22.5	13	13
15	.509	48	22.5	14	14
16	.717	40	22.5	15	15

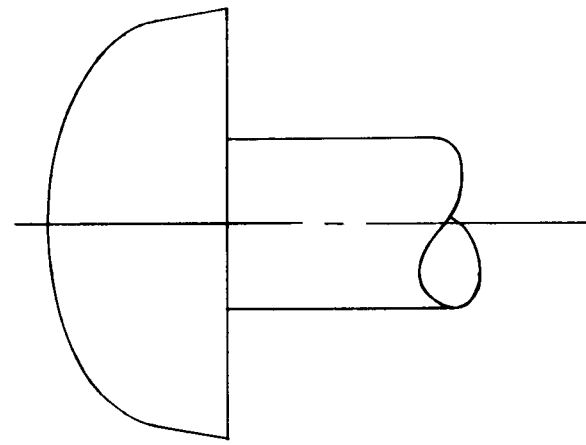

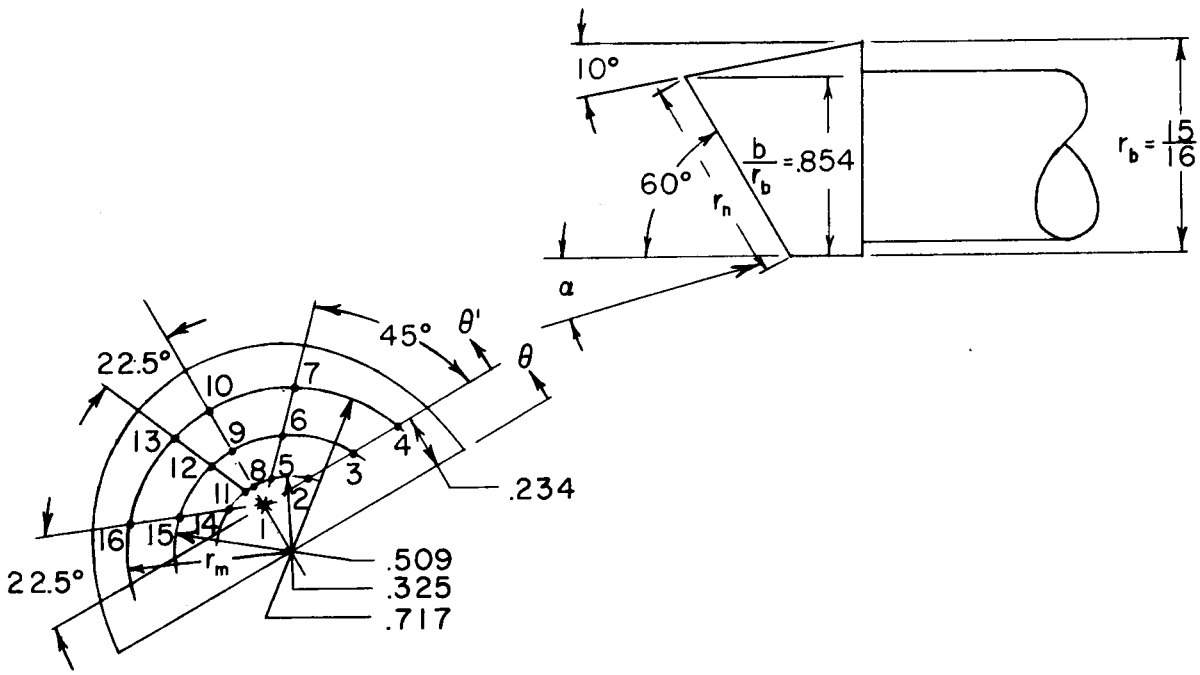

Figure 1.- Geometry and instrumentation of model (all dimensions in inches).

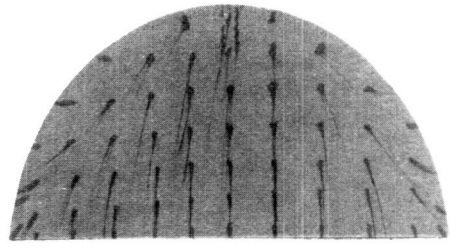

$\alpha = 0°$

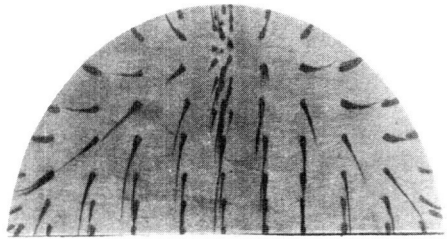

$\alpha = 10°$

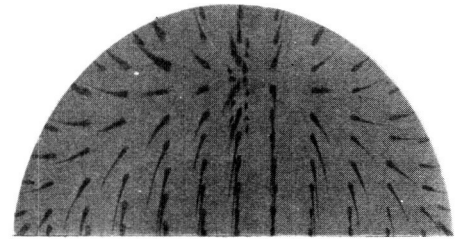

$\alpha = 20°$

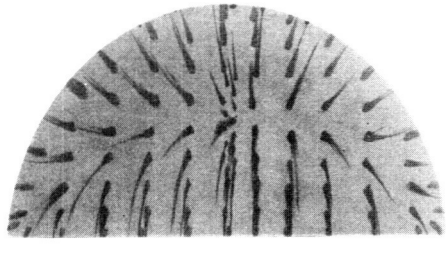

$\alpha = 30°$

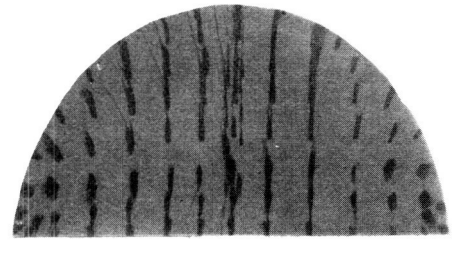

$\alpha = 40°$

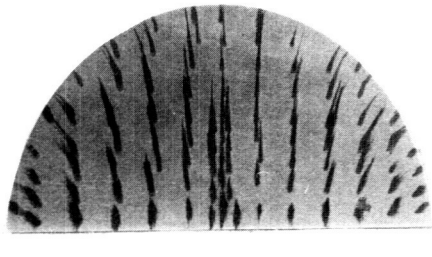

$\alpha = 50°$

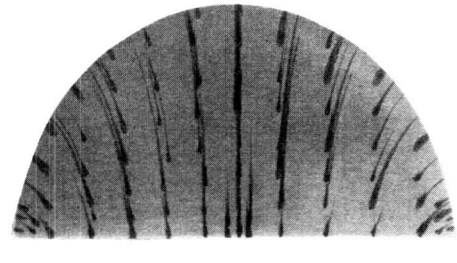

$\alpha = 60°$

L-63-16

Figure 2.- Oil-flow patterns for test model at various angles of attack.

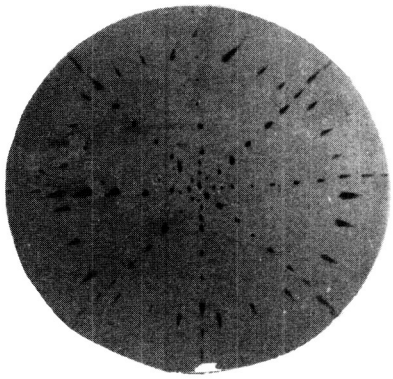

$\alpha = 0°$

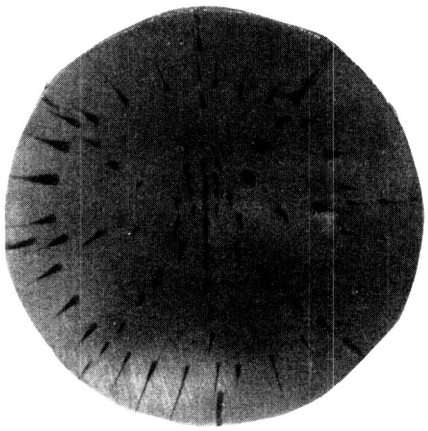

$\alpha = 5°$

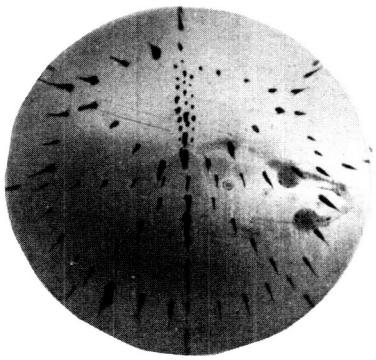

$\alpha = 15°$

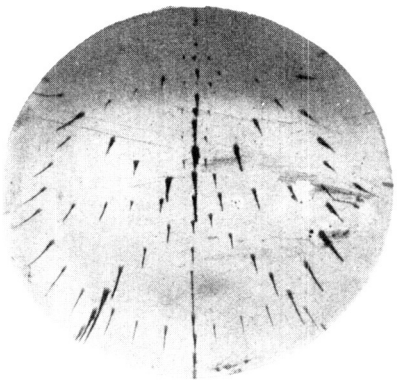

$\alpha = 20°$

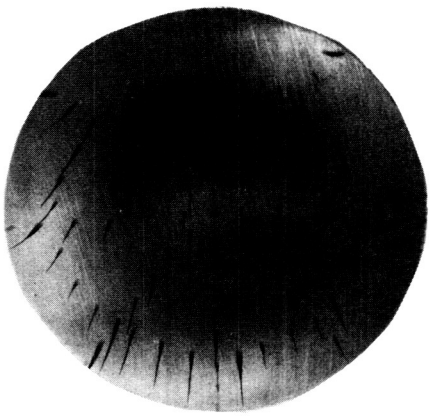

$\alpha = 30°$

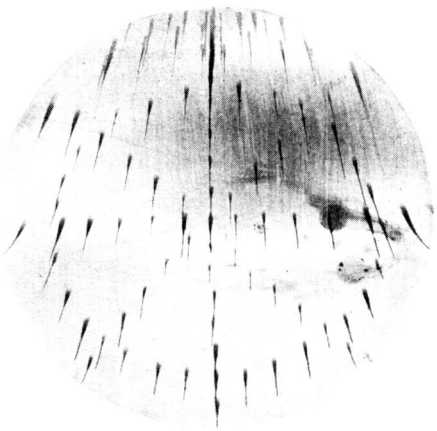

$\alpha = 45°$

L-63-17

Figure 3.- Oil-flow patterns for disk at various angles of attack. M = 8.

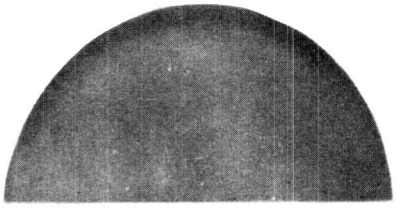

$\alpha = 0°$

$\alpha = 20°$

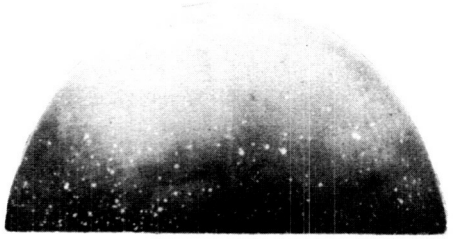

$\alpha = 40°$

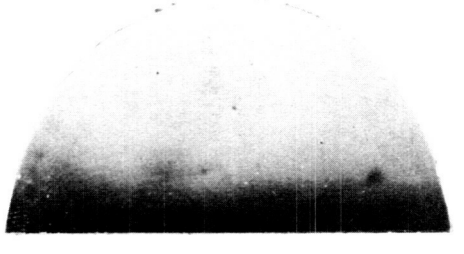

$\alpha = 60°$

L-63-18

Figure 4.- Temperature-sensitive-paint results for test model at various angles of attack.

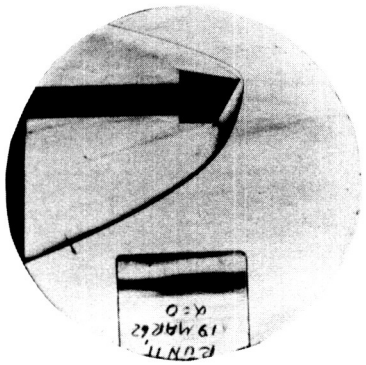

α = 0°

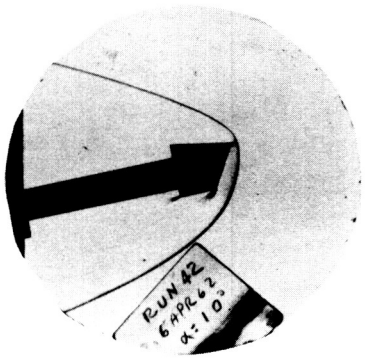

α = 10°

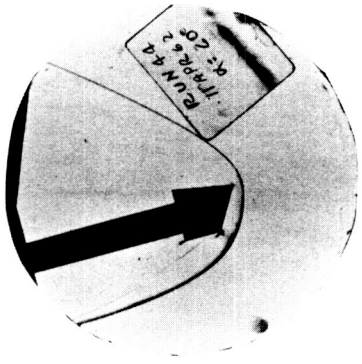

α = 20°

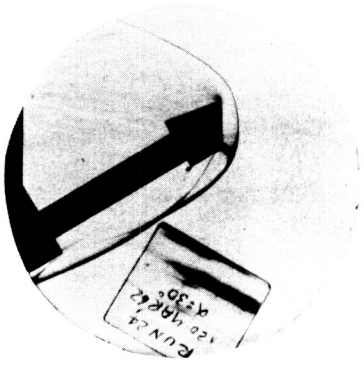

α = 30°

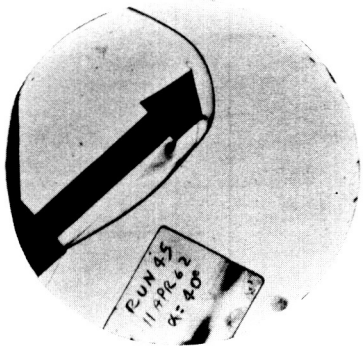

α = 40°

α = 50°

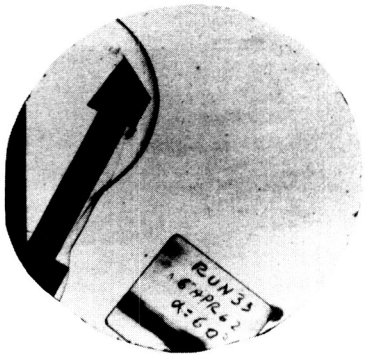

α = 60°

Figure 5.- Schlieren photographs of flow over test model. L-63-19

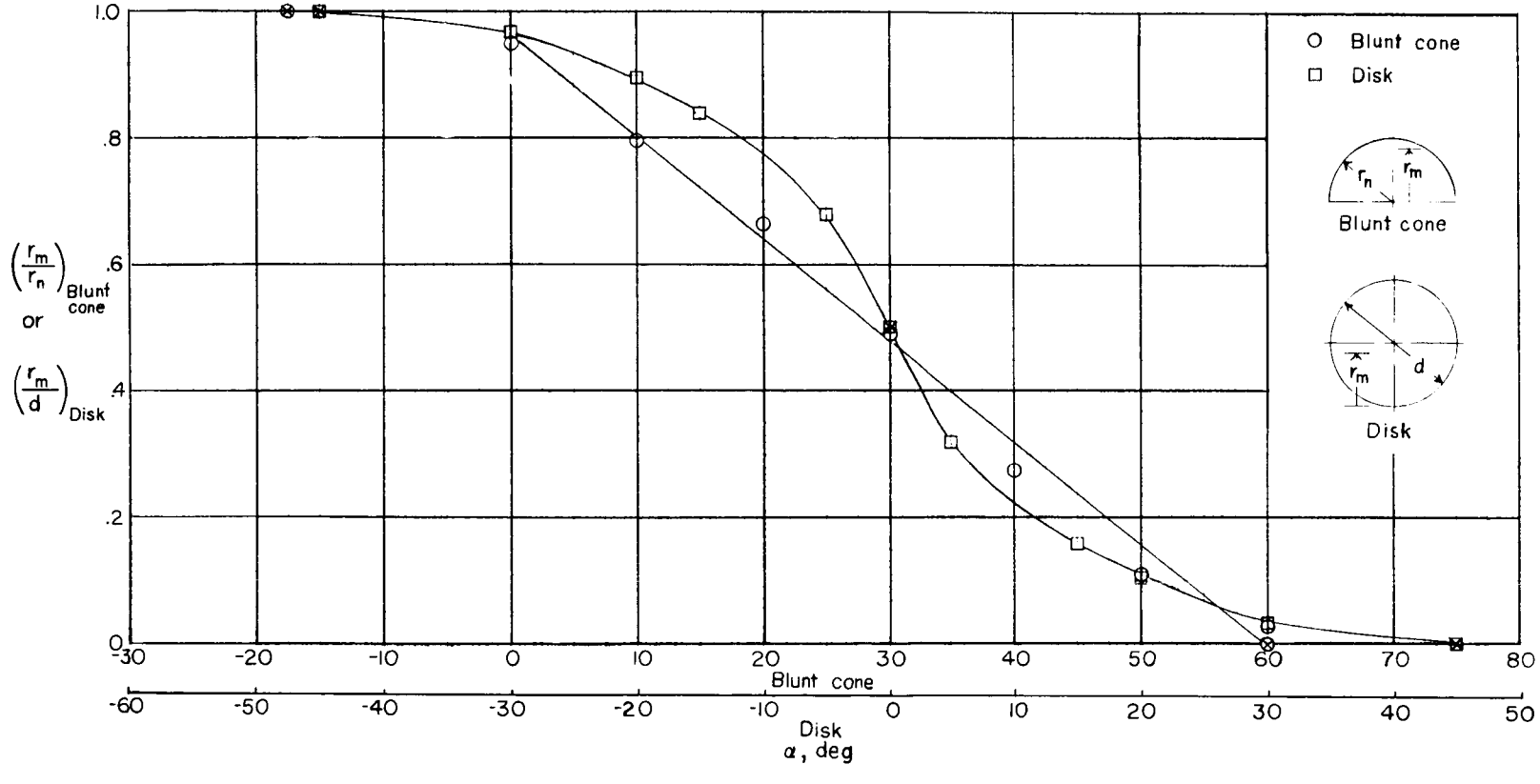

Figure 6.- Stagnation-point location obtained from oil-flow tests for various angles of attack. (The symbols ⊗ and ⊠ indicate estimated end points.)

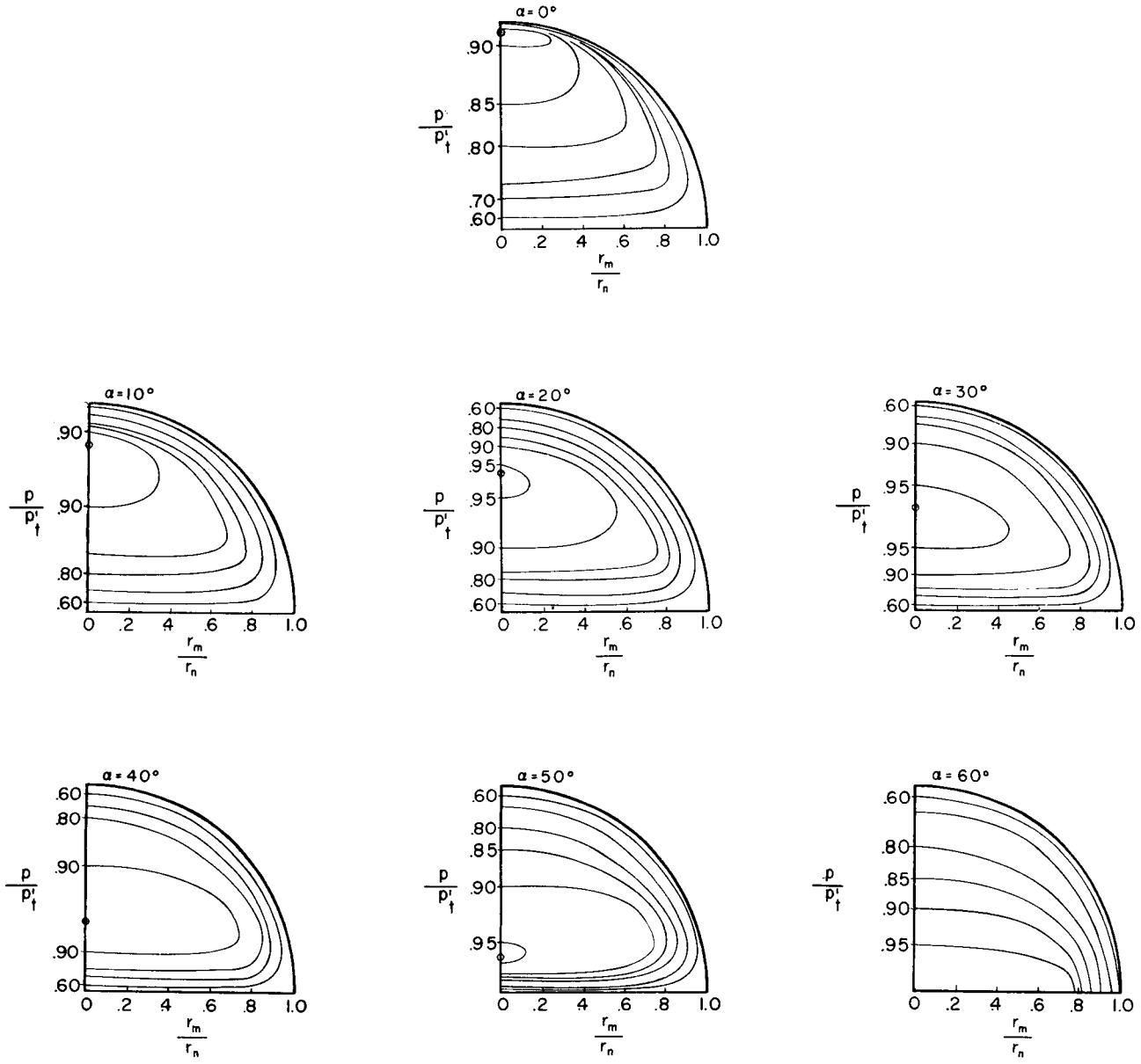

Figure 7.- Lines of constant pressure for test model at various angles of attack. (The symbol o indicates stagnation point.)

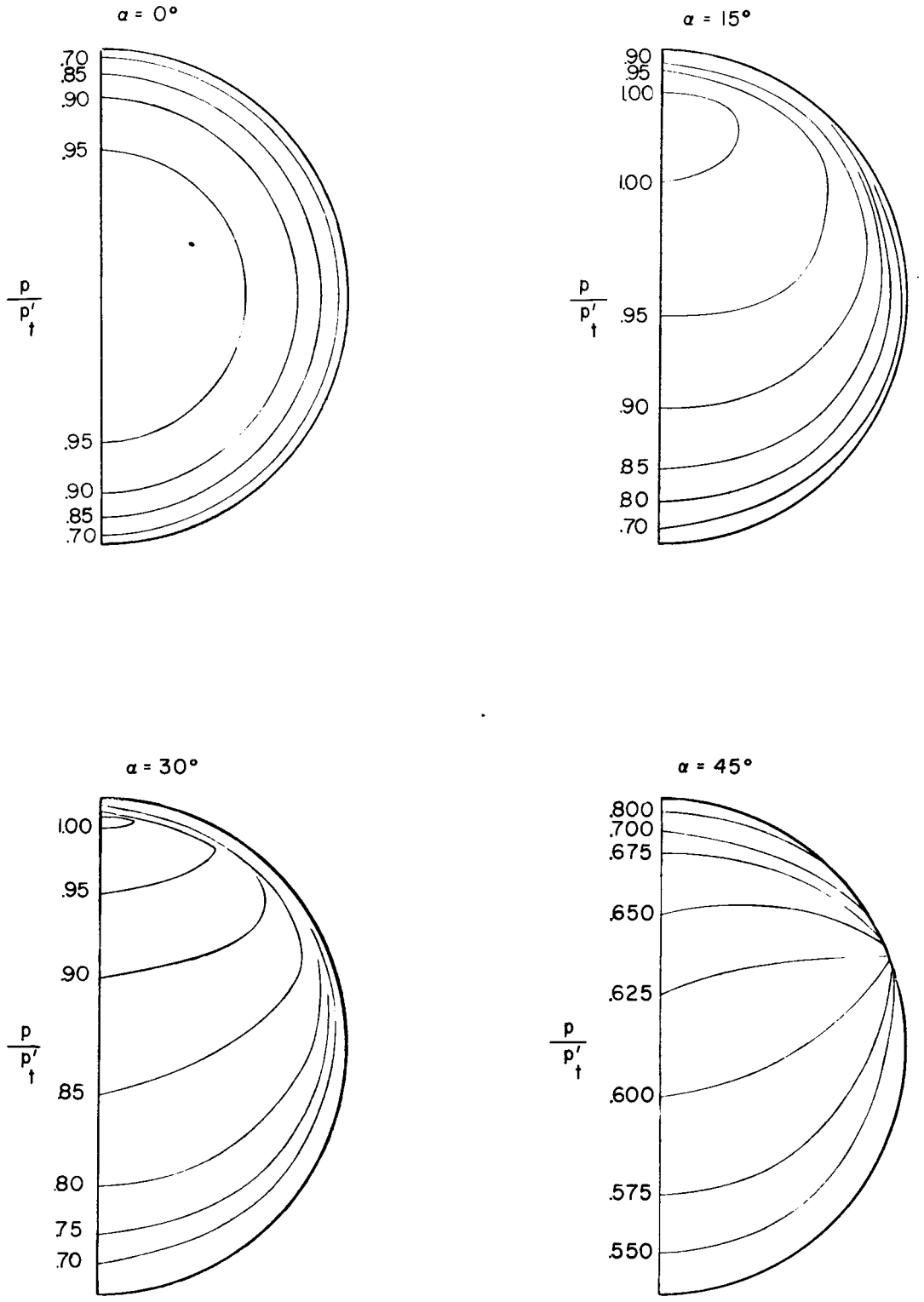

Figure 8.- Lines of constant pressure for disk at various angles of attack (from ref. 10).

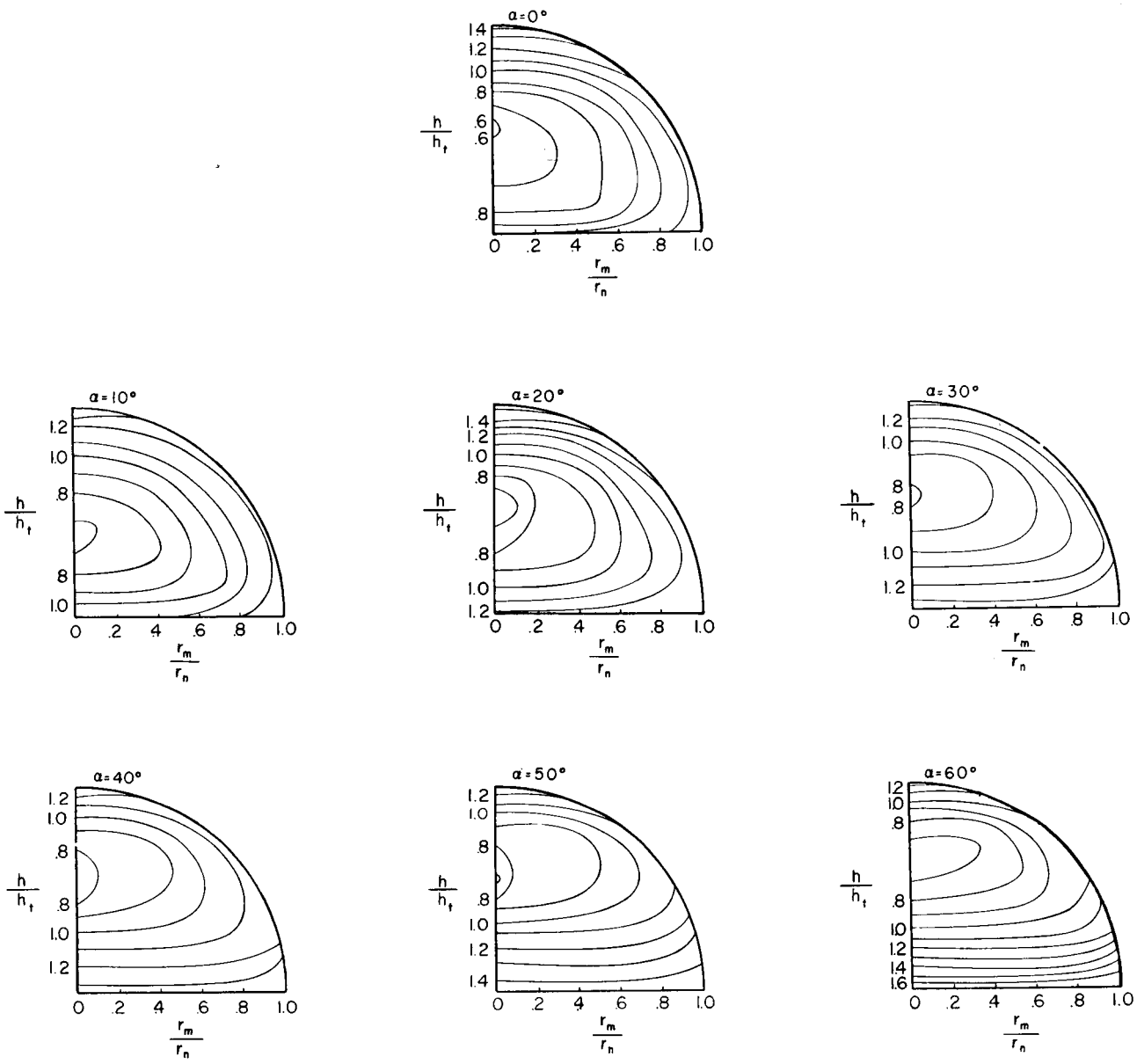

Figure 9.- Lines of constant heating for test model at various angles of attack.

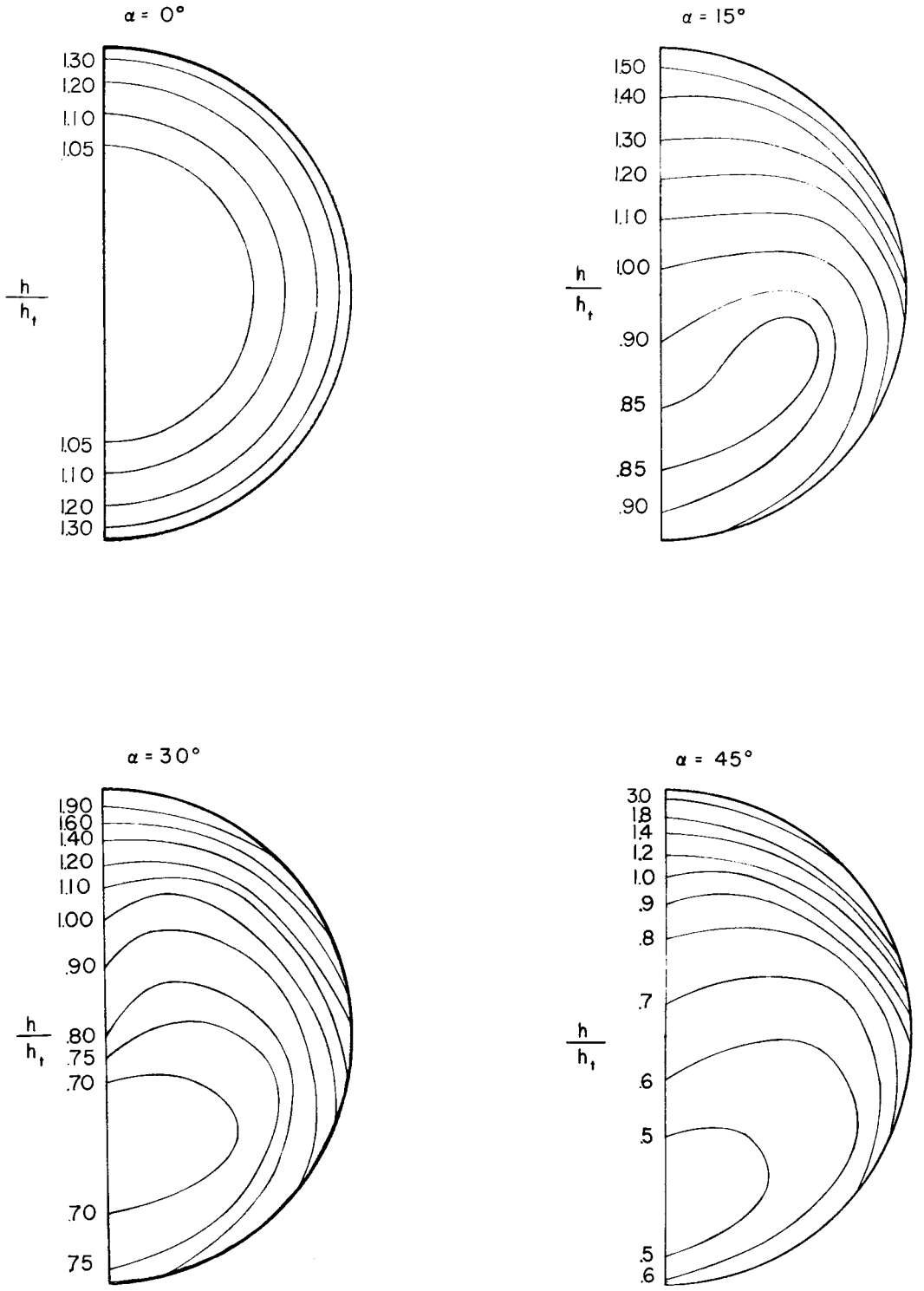

Figure 10.- Lines of constant heat-transfer coefficient for disk at various angles of attack (from ref. 10).

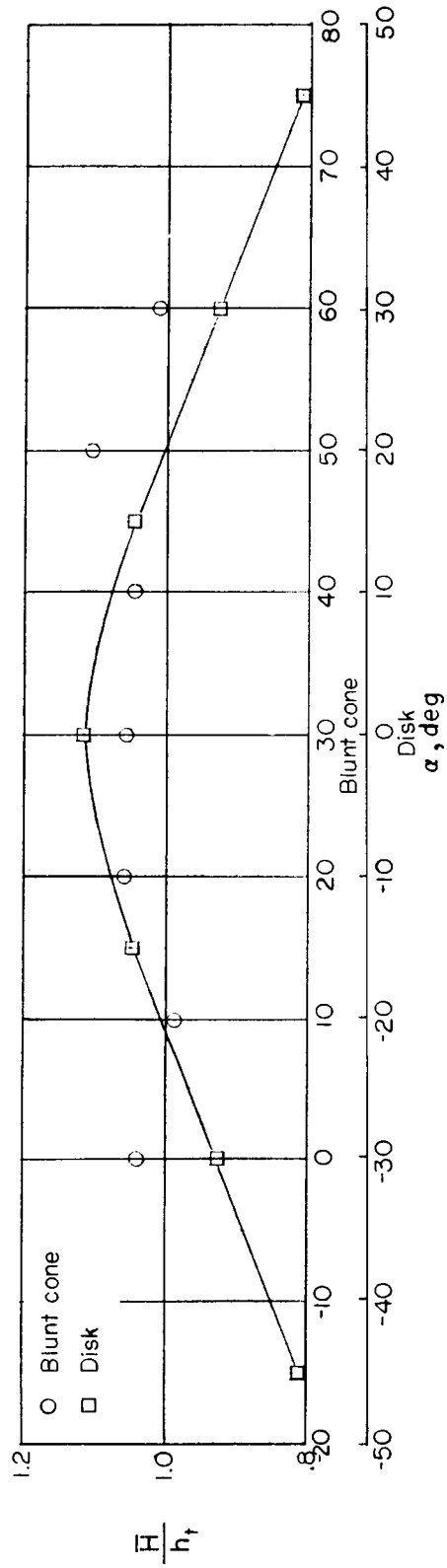

Figure 11.- Average heat-transfer coefficient for various angles of attack.